ULTRASONIC IMAGING **29,** 105-121 (2007)

# Effects of Phase Aberration and Noise on Extended High Frame Rate Imaging

JING WANG AND JIAN-YU LU

*Ultrasound Laboratory*
*Department of Bioengineering*
*The University of Toledo*
*Toledo, OH 43606*
*jilu@eng.utoledo.edu*

Based on the high frame rate (HFR) imaging theories, an extended HFR imaging method has been developed recently in our lab where multiple limited-diffraction array beams or steered plane waves are used in transmissions to reconstruct a high quality image of an equivalent dynamic focusing in both transmissions and receptions. The method has the potential to simplify imaging systems because the fast Fourier transform and square-wave aperture weightings can be used. The method is also flexible in using different numbers of transmissions for a continuous trade-off between image quality and frame rate. In this paper, we study the effects of phase aberration and noise on the extended HFR imaging method with *in vitro* experiments and compare the results with those obtained with a conventional delay-and-sum (D&S) method of a fixed-transmission focus and a dynamically-focused reception. In the experiments, an ATS539 tissue-mimicking phantom and an Acuson V2 phase array transducer (128 elements, 2.5 MHz, and 0.15-mm pitch) were used. The transducer was driven by a homemade general-purpose HFR imaging system that was capable of producing both the limited-diffraction array beams and steered plane waves and echo data were acquired with the same system and then transferred to a personal computer via a universal serial bus (USB) 2.0 link for image reconstructions. The phase aberration was introduced by adding random phase shifts to both transmission and reception beams. The random noise was added to the received radiofrequency echo data. Results show that the phase aberration and noise degrade both the extended HFR and the conventional delay-and-sum (D&S) imaging method. However, images reconstructed with the extended HFR imaging method have an overall higher quality than those with the D&S method given the phase aberration and noise models studied.

Key words: High-frame-rate imaging; limited-diffraction beams; noise; phase aberration; X waves.

## I. INTRODUCTION

In 1941, Stratton studied a Bessel beam that does not diffract in theory.[1] In 1987, Durnin studied the Bessel beam experimentally[2, 3] and termed it "nondiffracting beam" or "diffraction-free beam." Because any practical beams that are produced with a finite energy and aperture will eventually diffract, Durnin's terminologies were controversial and thus a new term "limited-diffraction beams" was used by us.[4] In 1991, new families of limited-diffraction beams called X waves were discovered.[5-8] Unlike the Bessel beams, X waves contain multiple frequencies and have the same phase and group velocities. In theory, limited-diffraction beams can propagate to an infinite distance without spreading. When these beams are produced with a finite aperture and energy, they have a large depth of field (i.e., they do not diffract over a large distance). Because of this property, limited-diffraction beams and



0161-7346/07 $18.00

other related beams have been studied extensively by many researchers in medical imaging,[9-12] tissue property identification,[13] nondestructive evaluation (NDE) of materials,[14] blood flow velocity[15] and velocity vector[16] imaging, fast ultrasound field computation for two-dimensional (2D) array transducers,[17] optical coherent tomography (OCT),[18] optical communications,[19] and optics[20] and physics[21] areas. The importance of these beams and their applications has also been reported by featured articles.[22-24]

Based on the X wave theories,[5-8] a two-dimensional (2D) and three-dimensional (3D) high frame rate (HFR) imaging method was developed in 1997.[25-27] This method uses the fast Fourier transform (FFT) to reconstruct images and thus reduces computations and may simplify imaging systems. Recently, the method has been extended to include various transmission schemes,[28-30] such as multiple limited-diffraction array beam[31, 32] and steered plane wave[33-35] transmissions. Multiple transmissions increase image signal-to-noise ratio (SNR), resolution and contrast over a large field of view, achieving an equivalent dynamic focusing in both transmissions and receptions.[28-30] This allows a continuous trade-off between image quality and frame rate for various medical applications. In addition, square-waves, instead of exact sine and cosine aperture weightings, can be applied to limited-diffraction array beam transmissions[28] and receptions[36] to further improve the image quality and simplify imaging systems.

Phase aberration of biological soft tissues and signal noise of imaging systems are two major limiting factors on the quality of medical ultrasound imaging. The phase aberration is due to an error of an assumption of speed of sound of objects to be imaged (first-order) and/or variations of the speed of sound in inhomogeneous objects (second order). The phase aberration distorts wave fronts and introduces errors in beamforming, lowering image contrast and resolution. In transmission, the phase aberration affects beam focusing and steering. In reception, it causes misalignment of echo signals and diminishes the signals in coherent summations of image reconstructions. In addition to the phase aberration, the signal noise of imaging systems is another source of distortions that degrades the image quality by lowering the SNR and image contrast. Because ultrasound signals are attenuated exponentially with the increase of propagation distances, the noise limits the depth where usable ultrasound images can be reconstructed.

Because both the phase aberration and noise degrade image qualities and may cause inaccurate clinical interpretations of images, many researchers have studied their effects on medical ultrasound imaging and proposed methods for the correction of the phase aberration and the reduction of noises. For example, Flax and O'Donnell used a cross-correlation peak to measure the difference of arrival time on transducer elements to get phase correction profiles to compensate for phase aberration.[37] Nock et al used a speckle brightness method to do a phase correction, where the signal from each element of the transducer was aligned relative to a summed signal of all elements.[38] Freiburger et al developed a local correlation and phase closure method, in which the local phase closure was enforced within 4-element loop to correct phase errors.[39] Rachlin tried to detect the difference of linear components in phase spectra of echoes and estimated phase correction profiles from the matrix of arrival time measurements.[40] Ng et al evaluated and reviewed several phase aberration correction algorithms.[41] To reduce image noises and improve the SNR of imaging systems, O'Donnell used a pseudo-chirp code excitation to increase the penetration of ultrasound.[42] Shen et al used a post-beamforming technique to enhance contrast resolutions.[43] Aussel and Monchalin applied a deconvolution technique to echo data to reduce structure noises.[44]

Although the effects of both the phase aberration[45] and noise[46] have been studied previously for the HFR imaging method[25-27] and have been compared with the conventional delay-and-sum (D&S)[47] method, they have not been studied for the extended HFR imaging methods.[28-30] In this paper, the effects of both the phase aberration and noise for the extended HFR imaging methods were studied with *in vitro* experiments on an ATS539 tissue-mimick-

ing phantom (ATS Laboratory, Inc.). The experiments were conducted with a homemade general-purpose HFR imaging system[28, 48, 49] and an Acuson V2 phased-array transducer (Acuson Corp., Mountain View, CA, USA) of 128 elements, 2.5-MHz center frequency, and 0.15-mm pitch. The phase aberration was introduced by adding random phase shifts (phase screens) to both transmission and reception beams. The random noise was added to the received radiofrequency (rf) echo data. For comparison, experiments were also conducted with the conventional D&S method of a fixed transmission focus of 70 mm and a dynamically-focused reception. Results show that both the phase aberration and noise degrade the quality of both the extended HFR imaging and the conventional D&S methods. However, the overall quality of images reconstructed with the extended HFR imaging method is higher than that of the D&S method under the same phase aberration and noise conditions and the models studied. This demonstrates that the extended HFR imaging method could be a useful tool for medical ultrasound imaging.

## II. THEORY OF EXTENDED HFR IMAGING METHODS

### A. Theory

The following is a brief summary of the theory of the extended HFR imaging method[28-30] that is used to reconstruct images in this paper. Assuming that there is a 2D array transducer (a one-dimensional (1D) array is a special case of a 2D array) and the transducer is weighted with a limited-diffraction array beam, ${}^{R}_{Array}(\vec{r}_0, t)$[25-27,31, 32], for a point scatterer located at $\vec{r}_0 = (x_0, y_0, z_0)$ that is illuminated by a wave, ${}^{T}_{Array}(\vec{r}_0, t)$, produced with the same transducer, ignoring multiple scattering (Born approximation),[50, 51] one obtains an echo signal from all the scatterers within a volume, $V$ (see Eq. (8) of reference 28):

$$
\begin{aligned}
& R_{k_{x_R}\ k_{x_T}, k_{y_R}\ k_{y_T}}(t) \\
& \quad {}_{V} f(\vec{r}_0)[\ {}^{T}_{Array}(\vec{r}_0, t) * \ {}^{R}_{Array}(\vec{r}_0, t)]d\vec{r}_0 \\
& \quad \frac{1}{2}\ \frac{A(k)T(k)H(k)}{c}\ {}_{V} f(\vec{r}_0) e^{i(k_{x_R}\ k_{x_T})x_0\ i(k_{y_R}\ k_{y_T})y_0\ i(k_{z_R}\ k_{z_T})z_0} d\vec{r}_0\ \ e^{\ i\ t} dk \\
& \quad \frac{1}{2}\ \frac{A(k)T(k)H(k)}{c} F(k_{x_R}\ \ k_{x_T}, k_{y_R}\ \ k_{y_T}, k_{z_R}\ \ k_{z_T}) e^{\ i\ t} dk
\end{aligned}
\tag{1}
$$

where $f(\vec{r}_0)$ is an object function related to the scattering strength of the scatterers, $t$ is the time, $*$ represents convolution with respect to time and where (see Eqs. (6) and (7) of reference 28, respectively):

$$
{}^{T}_{Array}(\vec{r}_0, t)\ \ \frac{1}{2}\ \ A(k)H(k) e^{ik_{x_T}x_0\ \ ik_{y_T}y_0\ \ ik_{z_T}z_0} e^{\ i\ t} dk \tag{2}
$$

and

$$
{}^{R}_{Array}(\vec{r}_0, t)\ \ \frac{1}{2}\ \ T(k)H(k) e^{ik_{x_R}x_0\ \ ik_{y_R}y_0\ \ ik_{z_R}z_0} e^{\ i\ t} dk \tag{3}
$$

where $\vec{K}^R$ $(k_{x_R}, k_{y_R}, k_{z_R})$ and $\vec{K}^T$ $(k_{x_T}, k_{y_T}, k_{z_T})$ are the wave vectors of the array beams in reception and transmission, $k_{z_R}$ $\sqrt{k^2 \quad k_{x_R} \quad k_{y_R}}$ 0 and $k_{z_T}$ $\sqrt{k^2 \quad k_{x_T} \quad k_{y_T}}$ 0, where $k = /c$, $= 2 f$ is the angular frequency, $f$ is the frequency, $c$ is the speed of sound in the medium and where $k_{x_R}$, $k_{y_R}$, $k_{x_T}$ and $k_{y_T}$ are free parameters. $T(k)$ and $A(k)$ are the transfer functions[52] of the transducer for the reception and transmission, respectively, and $H(k)$ is the Heaviside step function.[53]

Taking a temporal Fourier transform of $R_{k_{x_R} \quad k_{xT}, k_{y_R} \quad k_{y_T}}(t)$ in Eq. (1) with respect to the time, $t$, one obtains a relationship between the temporal Fourier transform of received echo signal and the spatial Fourier transform of the object function (see Eqs. (8) and (9) of reference 28):

$$\tilde{R}_{k_x^{'}, k_y^{'}}( \quad ) \quad \frac{A(k)T(k)H(k)}{c^2} F(k_x^{'}, k_y^{'}, k_z^{'}) \tag{4}$$

where

$$\begin{array}{ccccc} k_x^{'} & k_{x_R} & k_{x_T} & & \\ k_y^{'} & k_{y_R} & k_{y_T} & & \\ k_z^{'} & k_{z_R} & k_{z_T} & \sqrt{k^2 \quad k_{x_R}^2 \quad k_{y_R}^2} & \sqrt{k^2 \quad k_{x_T}^2 \quad k_{y_T}^2} \quad 0 \end{array} \tag{5}$$

and $\tilde{R}_{k_x^{'}, k_y^{'}}( \quad )$ and $R_{k_{x_R} \quad k_{xT}, k_{y_R} \quad k_{y_T}}(t)$ are a Fourier transform pair and $F(k_x^{'}, k_y^{'}, k_z^{'})$ is a 3D spatial Fourier transform of the object function, $f(\vec{r}_0)$. Because of the relationship between a limited-diffraction array beam aperture weighting and a 2D Fourier transform of echo signals of transducer elements over the same transducer aperture,[28] $\tilde{R}_{k_x^{'}, k_y^{'}}( \quad )$ is the same as a 3D Fourier transform of the echo signal over both the transducer aperture and time.

In the following, a 2D version of Eqs. (4) and (5) (simply setting $k_{y_T} \quad k_{y_R}$ 0) will be used for the reconstructions of images with the extended HFR imaging method through an inverse Fourier transform of $F(k_x^{'}, k_z^{'})$.[28]

### B. Image reconstruction methods

To reconstruct images with the extended HFR imaging method, two transmission scenarios were used. One was with limited-diffraction array beams[31-32] and the other was with steered plane waves. To acquire data, an Acuson V2 transducer was used, which is a 1D array with 128 elements, 2.5-MHz center frequency, 0.15-mm pitch, and 14-mm elevation dimension of a fixed 68-mm elevation focal length. To reconstruct images, the minimum and maximum frequencies were set to 0 and 5 MHz, respectively.[28] For limited-diffraction array beam transmissions, the free parameter, $k_{x_T}$, was equally spaced from 0 to $k_{x_T \max}$, where $k_{x_T \max} = k_c \sin( /4)$ and $k_c = 2 f_c/c$, and where $f_c$ was the center frequency of the transducer and $/4$ was a specified maximum equivalent steering angle off the axis of the transducer at the center frequency. For each $k_{x_T}$, both sine and cosine aperture weightings with a square-wave approximation were applied (see Eq. (16) of reference 28). Setting five steps of $k_{x_T}$, one obtains a total of 11 transmissions (one for a cosine weighting at $k_{x_T} = 0$, 5 for cosine weightings at other $k_{x_T}$, and another five for sine weightings corresponding to the cosine weightings). For 91 transmissions, there were 45 steps of $k_{x_T}$. Both 11 and 91 transmissions were used in the image reconstructions and both of which had the same field of view that was

larger than 45 . For each pair of sine and cosine transmissions, two areas of the coverage of $F(k_x', k_z')$ were obtained (see Eq. (16) in reference 28). The final image was obtained by coherently summing the sub-images reconstructed from the partial coverage of $F(k_x', k_z')$.[28] The coherent superposition increased the image resolution, contrast, field of view and SNR. The image quality was improved as the number of transmissions increased. To obtain the Fourier-space coverage, a relationship between the coordinates of the echo Fourier domain, $\tilde{R}_{k_x', k_y'}$ ( ), and the spatial Fourier domain of the object function, $F(k_x', k_z')$, was used:[29, 30]

$$k \quad \frac{k_{x_R} \quad k_x' \quad k_{x_T} \quad \sqrt{k_z'^2 \quad k_{x_T}^2 \quad k_x' \quad k_{x_T}^{\ 2\ 2} \quad 4k_z'^2 \quad k_x' \quad k_{x_T}^{\ 2}}}{2k_z'} \tag{6}$$

For steered plane wave transmissions,[25-27, 33-35] linear time delays were applied to the transmission signals along transducer elements:

$$(x_1) \qquad x_1 \sin \ _T / c \tag{7}$$

where $x_1$ (-*D*/2,*D*/2) is the position of the center of an element of the transducer, *D* is the aperture size of the transducer, and $_T$ is the steering or Axicon angle of an X wave[5-8] (see also Eq. (2) of reference 28) that was fixed for each transmission. The steering angle was changed from - /4 to /4 in 11 and 91 equally-spaced steps for 11 and 91 transmissions, respectively. From each transmission, an area in the spatial Fourier domain of the object function was covered through Eqs. (4) and (5). Images were reconstructed with a coherent superposition of all sub-images reconstructed from each transmission. Using a 2D case of Eq. (5), where $k_{x_T} = k\sin \ _T$, a relation between the coordinates of the echo Fourier domain and the spatial Fourier domain of the object function can be obtained[29, 30], which was used to reconstruct the images for steered plane wave transmissions in this paper:

$$k \quad \frac{k_{x_R} \quad k_x' \quad k \sin \ _T}{\dfrac{k_z'^2 \quad k_x'^2}{2k_z' \cos \ _T \quad 2k_x' \sin \ _T}} \tag{8}$$

For comparison, the conventional D&S method with a fixed transmission focal length of 70 mm and a dynamically-focused reception was also used to reconstruct images. In image reconstructions, 91 transmissions were produced with an evenly-spaced $\sin \ _T$,[28] where $_T$ was also ranged from - /4 to /4. This resulted in more transmissions at smaller steering angles than at larger ones. To reconstruct images of 11 transmissions with the D&S method, one out of every nine radial lines was extracted from the 91 transmissions over an image field of view of ± /4 and then the 11 lines were used to form an image with a bilinear interpolation. This approach shows that, when the image frame rate is increased (use only 11 transmissions) while maintaining a large field of view (e.g., ± /4), the extended HFR imaging method where a wide transmit beam is used outperforms the conventional D&S method where a tightly focused transmit beam is used. To avoid the degradation of image quality of

the D&S method, in most commercial imaging systems, either image depth or the field of view has to be reduced when the image frame rate is increased.

## III. EXPERIMENT CONDITIONS

### A. Experimental methods

To study the effects of the phase aberration and noise on the extended HFR imaging method with the limited-diffraction array beam and steered plane wave transmissions, *in vitro* experiments were performed with the homemade general-purpose HFR imaging system.[28, 48, 49] The system has 128 independent channels, each has a broadband (about 0.05-10 MHz) linear power amplifier in transmission and is capable of producing $\pm$144V arbitrary waveforms with a 40-MHz/12-bit digital-to-analog (D/A) converter on a 75- resistive load with a 6.25-ns time delay accuracy (the time-delay circuits use a 160-MHz clock). The system also has 128 independent high gain (up to 108 dB), low-noise, and wideband (about 0.25-10 MHz) time-gain-control (TGC) amplifiers. Echo signals from each receive channel are digitized with a 40-MHz/12-bit analog-to-digital (A/D) converter and stored in an SDRAM of up to 512 MB. Data are transferred to a personal computer (PC) via a universal serial bus (USB) 2.0 port for image reconstructions and the system is controlled with the same PC via the same USB link.[28]

In the experiments, the transducer described in the previous section was used. A one-cycle sine wave pulse at the center frequency (2.5 MHz) was used to excite the transducer and the time between adjacent transmissions was 187 *s*, which gave a maximum image frame rate of 486 and 59 frames/s for 11 and 91 transmissions, respectively. The rf echo signals were received with the same array and the signals were digitized at 40-MHz sampling rate and then down sampled to 10 MHz for the extended HFR imaging method to reduce computations in image reconstructions. The down sampling was possible because the echo signals were Fourier transformed with FFT (see Eq. (4)) in the extended HFR imaging method and the maximum frequency was 5 MHz. All frequency components beyond 5 MHz were ignored (filtered out) and thus 10 MHz sampling rate was adequate. For the D&S method, the sampling rate remained at 40 MHz so that the delay computation would be accurate.

An ATS539 multifunction tissue-mimicking phantom was used in the experiments. A cross-sectional structure of the phantom and the area for imaging are shown in figure 1. The phantom has a 0.5 dB/cm/MHz attenuation and a speed of sound of 1,450 m/s. The imaging area contains both line and cylindrical cystic targets. The diameter of the monofilament nylon wire targets is 0.12 mm and the diameters of the anechoic cylindrical cysts are 8, 6, 4, 3, and 2 mm (from left to right), respectively.

### B. Phase-aberration experiments

The phase aberration is a source of distortion in image reconstructions. Although the phase aberration was studied in detail previously[45] for the HFR imaging method with a single plane wave transmission at $_T = 0$,[25-27] it has not been studied for the extended HFR imaging method where partially reconstructed images are superposed coherently to form a final image. In medical imaging, the phase aberration is most severe in fat layers near the surface of transducers. Therefore, in this study, we assume that the phase aberration causes only time shifts in both transmission and reception beams. We also assume that the phase shift profiles across the transducer array elements are given by those in figure 2,[45] which were obtained by filtering a pseudo-random sequence with a spatial low-pass filter of a cut-off frequency of

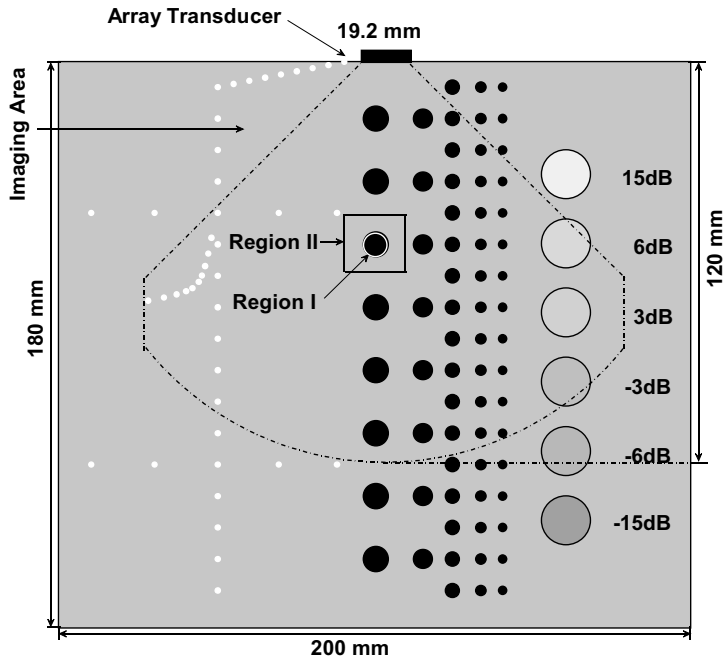


**FIG. 1** Cross section and imaging areas of an ATS539 multipurpose tissue-mimicking phantom (ATS Laboratories, Inc.). The fan-shaped area (bounded by dashed lines) indicates the imaging area. Regions I (circular with 6.3-mm diameter and concentric with the cyst) and II (square with 19 mm on each side but excluding the circle) represent the cystic and background areas for the computation of contrasts of the cyst. The center of the cyst is at about 55.2 mm from the surface and the cyst has a diameter of 8 mm.

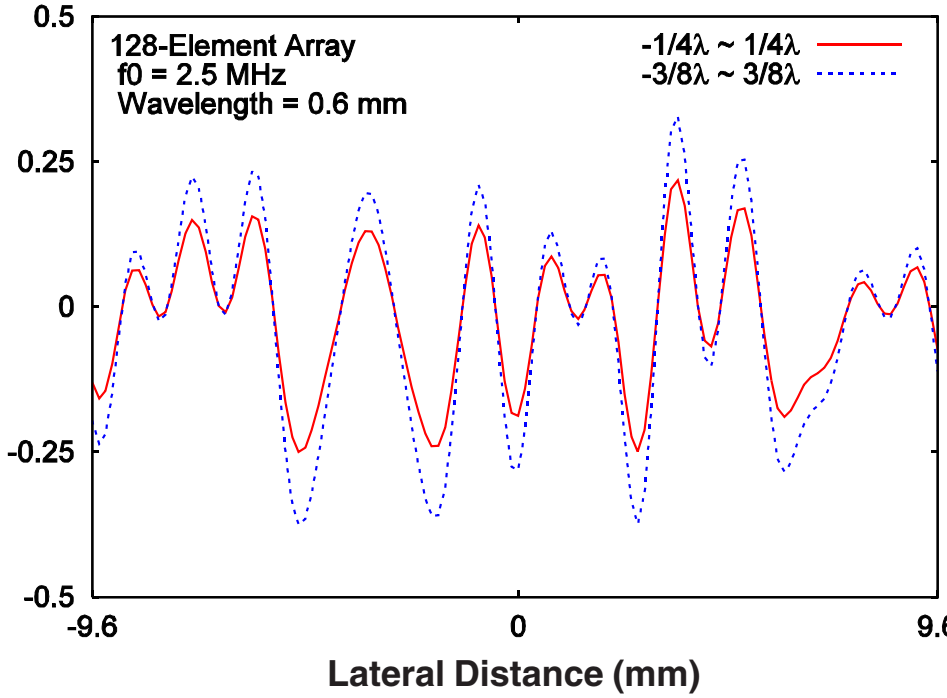


**FIG. 2** Two-phase screens with random phase distributions. The same phase screens were applied to both transmissions and receptions in the experiments. The first (solid line) and the second (dotted line) phase screens have maximum phase shifts of /2 and 3 /4, respectively, where = 0.6 mm is the wavelength. The transducer aperture is 19.2 mm, which is also the width of the phase screens. The phase screen has a maximum spatial frequency of .

about , where = 0.6 mm was the center wavelength of the transducer. The ranges of the phase shifts of the phase profiles were ±0.25 (or ±0.5 ) and ±0.375 (or ±0.75 ), respectively. To introduce the phase aberration in the experiment, the imaging system was programmed to delay transmission pulse for each transducer element according to the phase profile using one of the phase shift ranges. For each image reconstruction, all transmissions and receptions used the same phase profile and the shift range, which is the case in practical medical imaging. The flexibility of our imaging system has allowed us to do the experiments without using a physical phase screen and given us an opportunity to study the effects of different phase screens on the extended HFR imaging method in the future. However, a physical phase screen may allow one to study phase distortions that is originated some distance from the surface of a transducer.

### C. Noise experiments

In addition to the phase aberration, noise of an imaging system may reduce the image quality.[46] In a real imaging system, noise problems are complicated. There are many sources of noises and each may have different statistical characteristics and effects on image reconstructions. However, in this paper, we will only study the effects of a bandpass random noise of a fixed amplitude over the entire imaging depth. In the experiments, a pseudo-random sequence was first produced by a computer. Then, the sequence was filtered with a bandpass filter of a -6 dB bandwidth of about 81% of the center frequency of the transducer (used a Blackman window as the filter[5, 25] to mimic a bandpassed nature of the transducer and the matched bandpass filter of commercial imaging systems). Furthermore, the noise was assumed to have a fixed amplitude for echoes returned from all depths and was added to the rf echo signals after the TGC amplifiers. This maintained about the same SNR due to the added noise for all depths. The peak amplitudes of the noise were set to be 25% and 50%, respectively, relative to the peak values of the echo signals (notice that although the choices of the peak amplitude ratios were arbitrary, they were used consistently for all the imaging methods for which comparisons were made to support the conclusions of the paper). Due to the leaking of transmission signals into the receivers through the transmit/receive (T/R) switches, the peak value of the echo signals from each transducer element was about the same and was given by the saturated values near the surface of the transducer. Because of the TGC, the echoes have more or less the same amplitude for the entire imaging depth and for all of the 128 receive channels in all experiments. Therefore, the SNR was roughly determined by the ratio of the peak amplitude of the echo signals to the peak noise amplitude. Images were then reconstructed with the noise added echoes using the methods given in the previous section. The experiments had also naturally included the noise from the imaging system itself, which degraded image quality at a deeper depth.

It should be noticed that this simplified noise model would not affect the ability to assess the effects of noise on various image reconstruction methods since the results can always be compared at the same depths, although the added noise could be reduced in depths that are closer to the transducer surface due to smaller TGC gains. In practical imaging system, the SNR at deeper depths are of most concerns because signals may be attenuated heavily at those depths.

## IV. RESULTS

Images reconstructed with the limited-diffraction array beam and the steered plane wave imaging with 11 and 91 transmissions under no phase shift, ±0.25 random shifts and

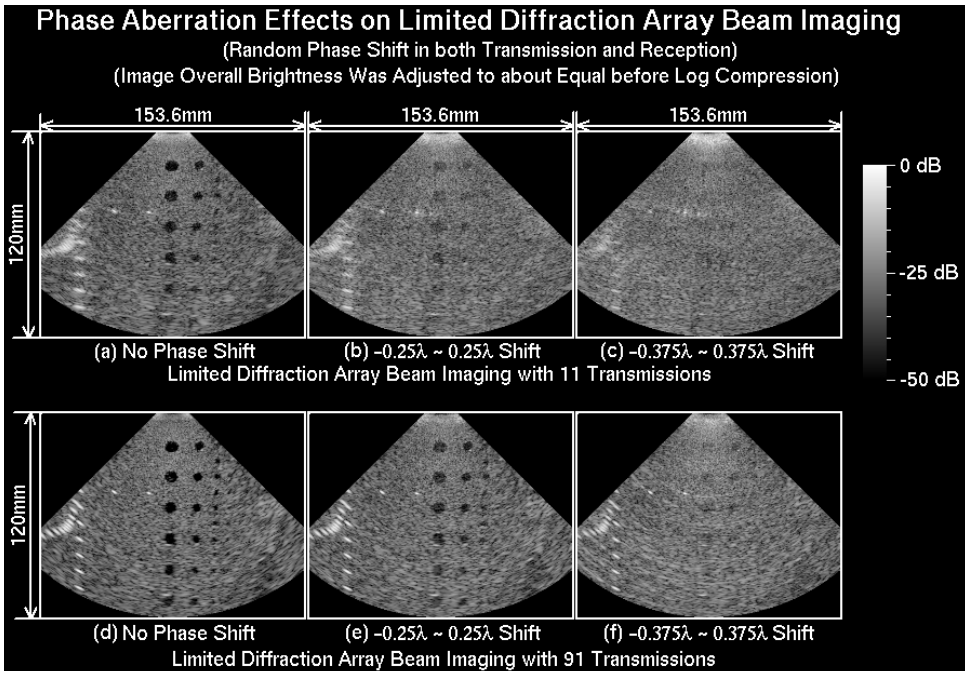


**FIG. 3** Results of *in vitro* experiments on an ATS539 tissue-mimicking phantom (see the imaging area shown in figure 1) with limited-diffraction array beam transmissions. An Acuson V2 phased array (128 elements, 2.5-MHz center frequency, 0.15-mm pitch, and 14-mm elevation aperture with a 68-mm elevation focal length) transducer and a homemade general-purpose high frame rate imaging system were used in the experiments. The phase screens in figure 2 were applied to the transducer elements in both transmissions and receptions. The speed of sound of the phantom was 1,450 m/s and the depth of images was 120 mm. Images were log-compressed with a dynamic range of 50 dB. The time between adjacent transmissions was 187 s. Panels (a), (b) and (c) represent images reconstructed with 11 transmissions (486 frames/s) after applying random phase screens of 0, -0.25 to 0.25 , and -0.375 to 0.375 maximum ranges of phase-shifts, respectively, where = 0.6 mm is the center wavelength. Panels (d), (e), and (f) are the same as panels (a), (b) and (c), respectively, except that they were reconstructed with 91 transmissions (59 frames/s).

$\pm 0.375$ random shifts are shown in figure 3 and figure 4, respectively. As a comparison, images reconstructed with the conventional D&S method with a transmission focal length of 70 mm and a dynamically-focused reception under the same conditions are shown in figure 5.

Results of the effects of the noise on the limited-diffraction array beam and steered plane-wave imaging are shown in figure 6 and figure 7, respectively. Similar to figure 5, images reconstructed with the D&S method under the same conditions of the noise are shown in figure 8 for comparison.

To study quantitatively the degradation of the contrast of an anechoic region due to the phase aberration or noise, the following formula was used to calculate the contrast:[45]

$$C_c \quad 20\log_{10}\frac{m_i}{m_o} \tag{9}$$

where $m_i$ and $m_o$ were mean values inside and outside of the envelope detected images of the cyst, respectively. For an anechoic region, an ideal imaging system would produce a contrast value of - according to Eq. (9). Any increase of $C_c$ is due to the imperfection of the imaging system.

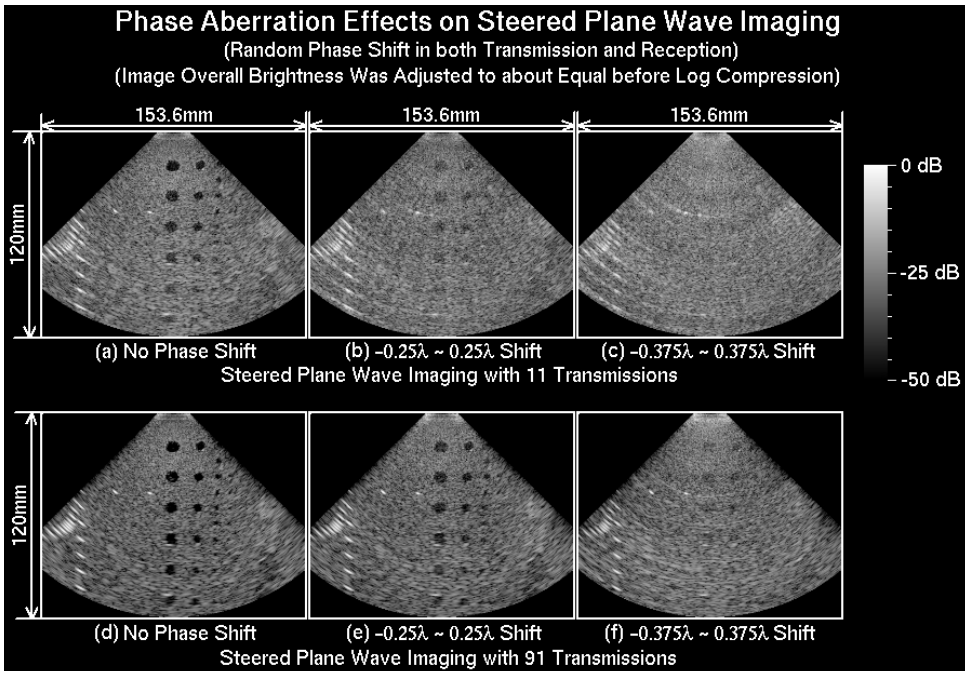


**FIG. 4** Same as figure 3 except that the steered plane waves, instead of the limited-diffraction array beams, were used in transmissions.

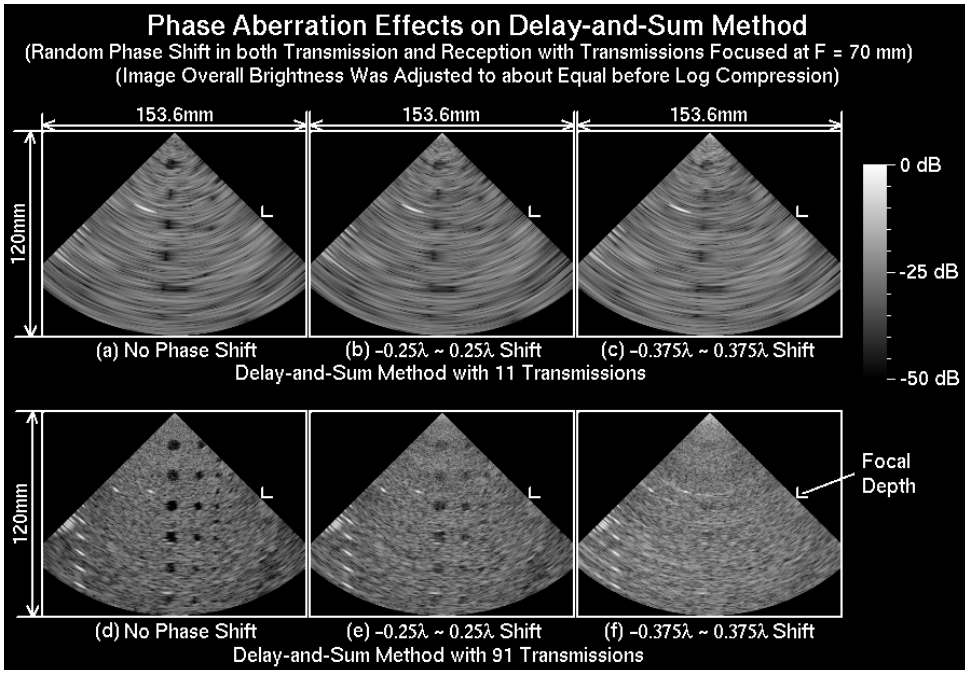


**FIG. 5** Same as figure 3 except that the delay-and-sum (D&S) method, instead of the limited-diffraction array beam imaging, was used for image reconstructions. The D&S method had a transmission focal length of 70 mm and a dynamically-focused reception. The focus is marked with a < sign in each panel. The results of 11 transmissions (top row) were obtained from those of 91 transmissions (bottom row) by evenly extracting each transmission out of every 9 over the 45 field of view and were produced with a bilinear interpolation.

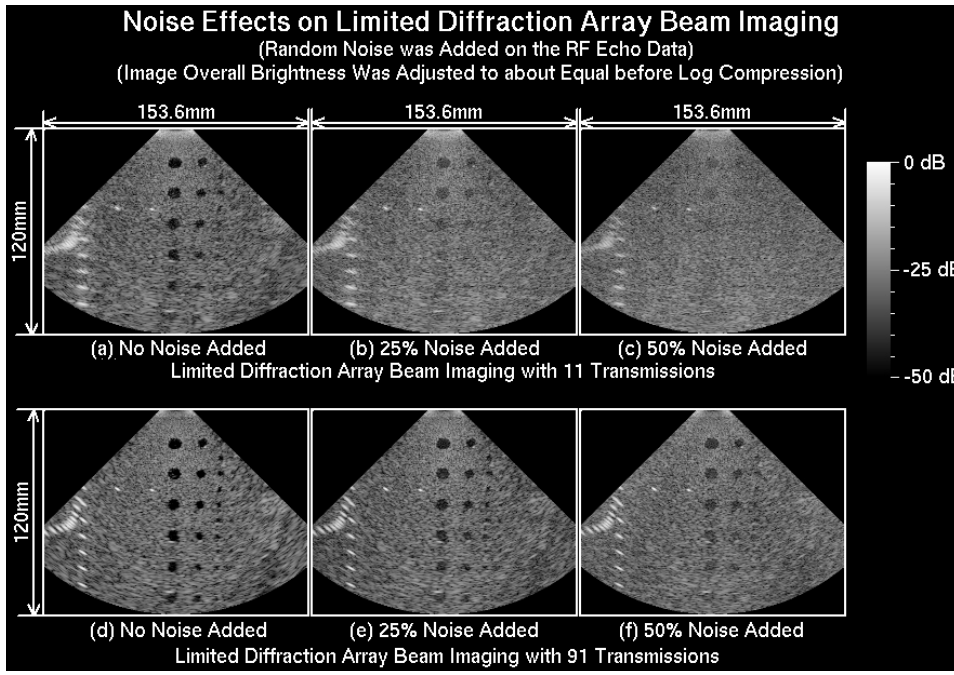


**FIG. 6** Effects of random noise of an imaging system on the limited-diffraction array beam imaging. The experiment conditions and the figure layout are the same as those of figure 3, except that a bandpass filtered random noise with peak amplitudes of 0% (panels (a) and (d)), 25% (panels (b) and (e)), and 50% (panels (c) and (f)) relative to the peak amplitudes of the received signals were added.

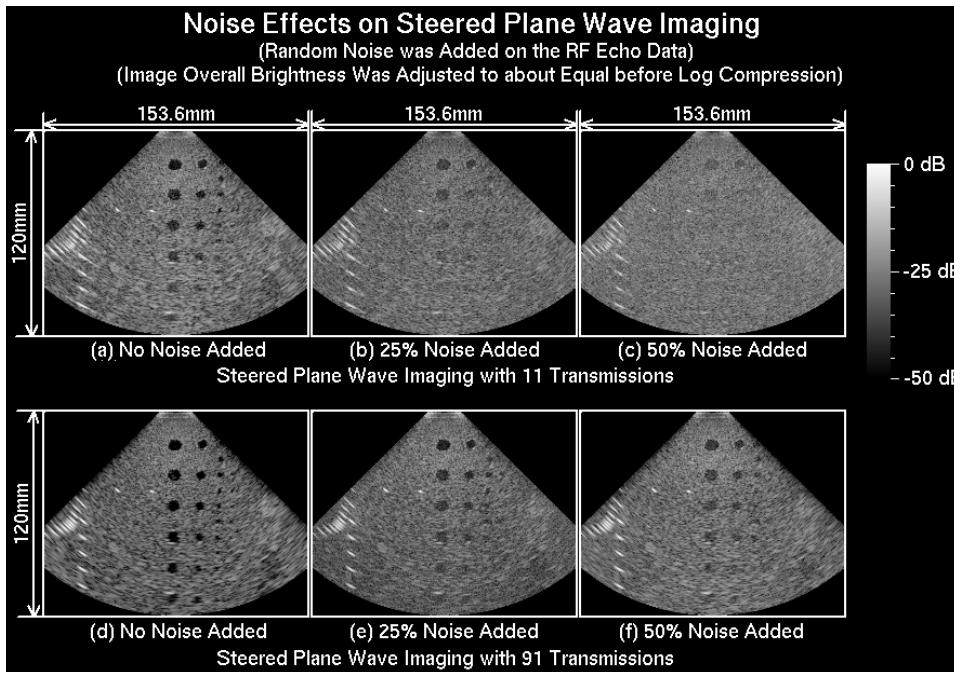


**FIG. 7** Same as figure 6 except that the steered plane waves, instead of the limited-diffraction array beams, were used in transmissions.

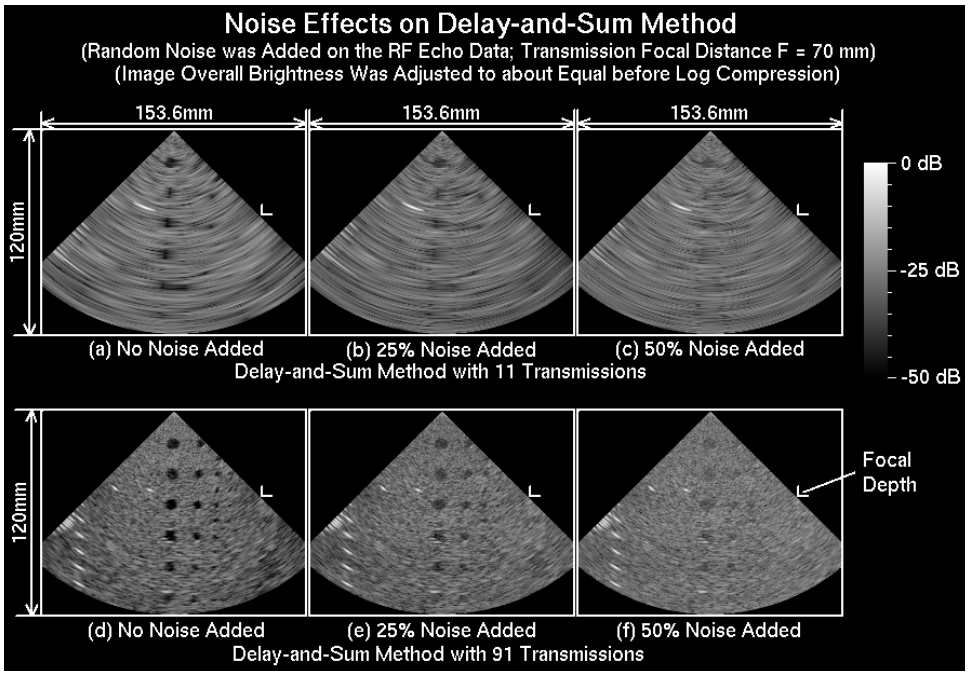


**FIG. 8** Same as figure 6 except that the delay-and-sum (D&S) method, instead of the limited-diffraction array beam imaging, was used for image reconstructions. The experiment conditions of the D&S method are the same as those of figure 5.

The areas for the calculations of $m_i$ and $m_o$ are shown in regions I and II, respectively, in figure 1. Region I has a diameter of 6.3 mm that is concentric with the cyst and region II is a square area with 19 mm on each side but excluding region I. The cystic target was located at about 55.2 mm in depth. The calculated contrasts for both the extended HFR imaging and the D&S methods are shown in figure 9.

## V. DISCUSSION

### A. Orders of phase aberrations

There are two orders of phase aberrations. One is an error of the assumption of the speed of sound of background tissues (first order) from the value of the speed of sound used in image reconstructions. The other is due to tissue inhomogeneity (second order). The second-order phase aberration is usually the main source of distortion in medical imaging. For most biological soft tissues, a speed of sound of 1,540 m/s is usually assumed. In this paper, only the second-order phase aberration was investigated and the speed of sound of the rubber-based ATS539 phantom was assumed to be 1,450 m/s which was given in the product specifications.

### B. Phase aberration models

Phase aberration models in biological soft tissues are complicated. Organs in the human body are not homogeneous in terms of the speed of sound. Moreover, refractions may occur on the boundaries between different organs or different structures within an organ. Therefore, a distributed phase aberration model would be more appropriate to characterize such

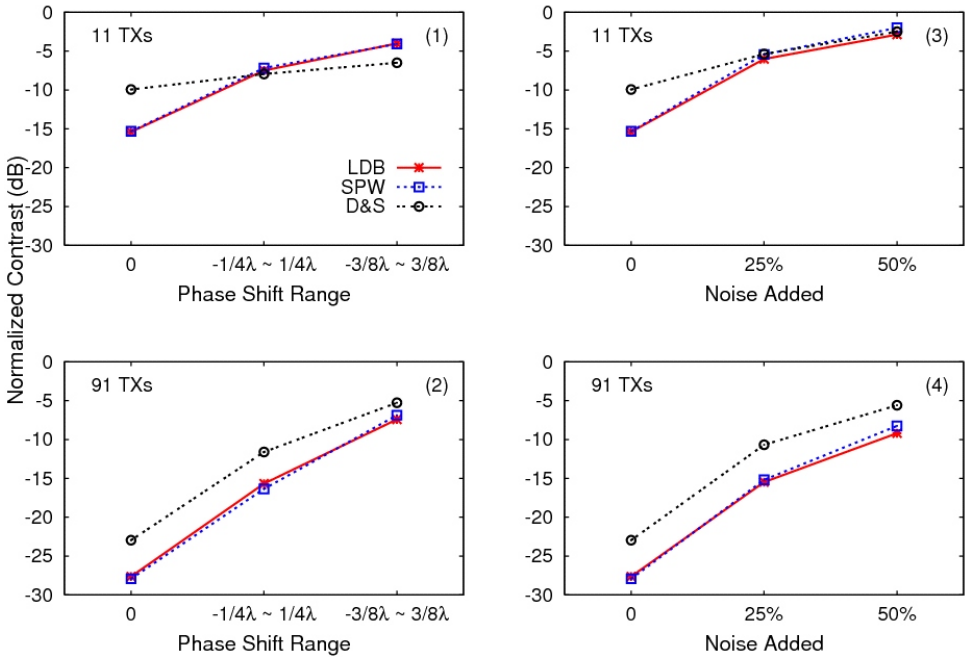


**FIG. 9** Comparison of contrasts of a cylindrical cystic target of an ATS539 multifunction tissue-mimicking phantom using regions I and II shown in figure 1 for the effects of the phase aberration (panels (1) and (2)) and noise (panels (3) and (4)) on different imaging methods. For a perfect imaging system, the cystic target should have a -dB contrast. Top two panels show results with 11 transmissions (TXs), while bottom two show those of 91 TXs. The solid lines with a 'star' symbol (red) represent the results of the limited-diffraction array beam (LDB) imaging; the dotted lines with 'square' symbol (blue) are the results of the steered plane wave (SPW) imaging; and the dotted lines with a 'circle' symbol (black) are those of the Delay-and-sum (D&S) method with transmission focal length of 70 mm and a dynamically focused reception.

distortions. However, in practice, it is difficult to compensate for a distributed phase aberration. Fortunately, the internal organs of human body usually have a relatively smaller phase aberration than that of the fat layers under the skin, which is near the surface of the transducer. Thus, a phase screen model is often used where the aberration layers of fat are simplified as a thin sheet of transparent but phase-shifting screen that is placed in front of the transducer, i.e., the phase aberration causes only random time shifts in both transmit and receive echoes. In this paper, only the phase screen model was used.

### C. Effects of phase aberration

The magnitude of phase aberration has a dramatic effect on the quality of reconstructed images. From figures 3-5, it is clear that for a peak-to-peak random phase shift magnitude of 0.5 center wavelengths across the transducer aperture of about 32 wavelengths, the image contrast is reduced significantly (see panels (b) and (e) in figures 3-5). As the magnitude increases to 0.75 center wavelengths, the image contrast is reduced further and the cystic targets are almost invisible (see panels (c) and (f) in figures 3-5). For the D&S method, the images reconstructed have a lower overall contrast as compared to those reconstructed with the limited-diffraction array beam and the steered plane wave methods using the same phase screens (compare the panels of figure 5 to the corresponding panels of figures. 3 and 4). This is because the images reconstructed with the D&S method of a fixed transmission focus and dynamically-focused reception does not have a very high overall quality as compared to those reconstructed with the extended HFR imaging method even without the phase aberra-

tion (compare panels (a) and (d) among figures 3-5). This observation is interesting because it demonstrates that for stationary objects,[54] the extended HFR imaging method produces higher quality images than the D&S method regardless of the phase aberration, in addition to many other advantages as mentioned before.[28]

In figure 9, it seems to indicate that the contrast of images reconstructed with the D&S method with 11 transmissions is higher than that with the extended HFR method. However, this is of little interest because with 11 transmissions, the image resolution of the D&S method is so poor that the object shapes are severely distorted (Figs. 3-5), which renders these images useless for medical diagnosis. This indicates that without using the wide transmit beams that are used in the extended HFR imaging method, the benefit of a tightly focused transmit beam of the conventional D&S method may be lost when image frame rate is increased while maintaining a large image depth and field of view.

### D. System noises

As mentioned before, the noise of an imaging system is complicated and may be described with different statistical models. In this paper, a simplified approach was used for a preliminary study of the effects of the noise, i.e., the noise was added to the echo signals after the signals were amplified by the TGC amplifiers. In practical imaging systems, TGC amplifiers precede A/D converters. Thus, such noise is equivalent to that produced at the input of the A/D converters. If the same amount of noise were added before the TGC amplifiers, the SNR would be further reduced for echoes returned from deeper depths due to the attenuation of ultrasound by tissues. Even though in our study the SNR is maintained about constant for all depths due to the TGC compensation, the effects of noise are still larger for object at deeper depths because of a reduced resolution and lowered contrast of the original images (Figs. 6-8). Despite of the simplified noise model, the comparison studies performed are valid because the noise added at different depths remains localized around the respective depths.

From the simplified model of the noise, it is found that the overall image quality is higher for the extended HFR imaging method as compared to that of the D&S under similar noise conditions (Figs. 6-8). The higher noise immunity may be due to the coherent summation used in the extended HFR imaging method.

As mentioned before, the comparison of the contrast of 11 transmissions shown in figure 9 (b) for the extended HFR imaging and the D&S method is not suitable for an assessment of the image quality because the quality of the images reconstructed with the D&S method is very poor.

### E. Extended HFR and D&S Imaging

From the experiment results, it is clear that in the absence of the phase aberration, noise, and motion,[54] the extended HFR imaging method produces higher quality images than the conventional D&S method with a fixed transmission focus of 70 mm and a dynamically-focused reception given the same number of transmissions (compare panels (a) and (d) among figures 3-8). In addition, as the number of transmissions increases, image quality is improved for all the methods (see panels (a) and (d) in figures 3-8). This is consistent with our previous studies.[28-30] Even with the phase aberration and noise, it is found that the extended HFR imaging method still outperforms the conventional D&S method in general. This may be because the extended HFR imaging method reconstructs higher-quality images to start with. It is worth noting that although the extended HFR imaging method lacks of transmission focusing in each transmission, which may reduce the SNR for each sub-image reconstructed from the transmission, the noise of the final images reconstructed is reduced significantly via the coherently superposition.

## VI. CONCLUSION

Recently, the 2D and 3D high frame rate (HFR) imaging method[25-27] was extended to include multiple transmissions with limited-diffraction array beams[31, 32] (or their square-wave approximations[28, 36]) and steered plane waves[33-35] to obtain high quality images of equivalent dynamic focusing in both transmissions and receptions.[28-30] In this paper, the effects of both the phase aberration and noise on the extended HFR imaging method have been studied with *in vitro* experiments on an ATS539 multipurpose tissue-mimicking phantom. The experiments were performed with a homemade general-purpose HFR imaging system[28, 48, 49] and an Acuson V2 128-element and 2.5-MHz phased array transducer and results are compared under the same conditions to those of the conventional delay-and-sum (D&S) method[47] with a transmission focus of 70 mm and a dynamically focused reception. The results show that images reconstructed with the extended HFR imaging method have a higher quality than those reconstructed with the D&S method, given the phase aberration and noise models studied. This may be due to the coherent superposition of multiple sub-images used in the extended HFR imaging method. This also demonstrates that, under the phase aberration and noise models studied, the extended HFR imaging method is superior to the conventional D&S method in terms of the image resolution, contrast and immunity to both phase aberration and noise effects for stationary objects,[54] in addition to having other advantages such as simplifying imaging systems.[28, 36]

## ACKNOWLEDGEMENTS

This work was supported in part by grant HL60301 from the National Institute of Health.

## REFERENCES

1. Stratton JA. *Electromagnetic Theory*, p. 356 (New York and London: McGraw-Hill Book Company, 1941).

2. Durnin J. Exact solutions for nondiffracting beams. I. The scalar theory, *J Opt Soc Am A. 4,* 651–654 (1987).

3. Durnin J, Miceli JJ, Jr., Eberly JH. Diffraction-free beams, *Phys Rev Lett 58,* 1499–1501 (1987).

4. Lu JY, Greenleaf JF. Sidelobe reduction for limited diffraction pulse-echo systems, *IEEE Trans Ultrason Ferroelec Freq Contr 40,* 735-746 (1993).

5. Lu JY, Greenleaf JF. Nondiffracting X waves - exact solutions to free-space scalar wave equation and their finite aperture realizations, *IEEE Trans Ultrason Ferroelec Freq Contr 39,* 19-31 (1992).

6. Lu JY, Greenleaf JF. Experimental verification of nondiffracting X waves, *IEEE Trans Ultrason Ferroelec Freq Contr 39,* 441-446 (1992).

7. Lu JY, Zou H, Greenleaf JF. A new approach to obtain limited diffraction beams, *IEEE Trans Ultrason Ferroelec Freq Contr 42,* 850-853 (1995).

8. Lu JY, Liu A. An X wave transform, *IEEE Trans Ultrason Ferroelec Freq Contr 47,* 1472-1481 (2000).

9. Lu JY, Greenleaf JF. Ultrasonic nondiffracting transducer for medical imaging, *IEEE Trans Ultrason Ferroelec Freq Contr 37,* 438-447 (1990).

10. Lu JY, Greenleaf JF. Pulse-echo imaging using a nondiffracting beam transducer, *Ultrasound Med Biol 17,* 265-281 (1991).

11. Lu JY, Zou H, Greenleaf JF. Biomedical ultrasound beam forming, *Ultrasound Med Biol 20,* 403-428 (1994).

12. Lu JY, Song TK, Kinnick RR, Greenleaf JF. In vitro and in vivo real-time imaging with ultrasonic limited diffraction beams, *IEEE Trans Med Imag 12*, 819-829 (1993).

13. Lu JY, Greenleaf JF. Evaluation of a nondiffracting transducer for tissue characterization, in *1990 IEEE Ultrason Symp Proc*, vol. 2, pp. 795-798 (IEEE Cat. no. 90CH2938-9, 1990) (ISSN: 1051-0117).

14. Lu JY, Greenleaf JF. Producing deep depth of field and depth-independent resolution in NDE with limited diffraction beams, *Ultrasonic Imaging 15,* 134-149 (1993).

15. Lu JY, Xu XL, Zou H, Greenleaf JF. Application of Bessel beam for Doppler velocity estimation, *IEEE Trans Ultrason Ferroelec Freq Contr 42,* 649-662 (1995).

16. Lu JY, Wang Z, and Kwon SJ. Blood flow velocity vector imaging with high frame rate imaging methods, in *2006 IEEE Ultrason Symp Proc,* vol. 2, pp. 963-966 (IEEE Catalog no. 06CH37777, 2006) (ISSN: 1051-0117).

17. Lu JY, Cheng J. Field computation for two-dimensional array transducers with limited diffraction array beams, *Ultrasonic Imaging 27,* 237-255 (2005).

18. Lu JY, Cheng J, Cameron B. Low sidelobe limited diffraction optical coherence tomography, in *Coherence Domain Optical Methods in Biomedical Science and Clinical Applications VI,* Tuchin VV, Izatt JA, Fujimoto JG, eds., *Proc SPIE,* vol. 4619, pp. 300-311(2002) (ISBN: 0-8194-4358-1).

19. Lu JY, He S. Optical X wave communications, *Opt Comm 161,* 187-192 (1999).

20. Trapani PD, Valiulis G, Piskarskas A, et al. Spontaneously generated X-shaped light bullets, *Phys Rev Lett 91,* 093904 (2003).

21. Conti C, Trillo S. Nonspreading wave packets in three dimensions formed by an ultracold Bose gas in an optical lattice, *Phys Rev Lett 92,* 120404 (2004).

22. Wade G. Human uses of ultrasound: ancient and modern, *Ultrasonics 38,* 1-5 (2000).

23. Wells PNT. Ultrasound imaging, *Phys Med Biol 51,* R83–R98 (2006).

24. Day C. Intense X-shaped pulses of light propagate without spreading in water and other dispersive media, *Phys Today 57,* 25-26 (2004).

25. Lu JY. 2D and 3D high frame rate imaging with limited diffraction beams, *IEEE Trans Ultrason Ferroelec Freq Contr 44,* 839-856 (1997).

26. Lu JY. Experimental study of high frame rate imaging with limited diffraction beams, *IEEE Trans Ultrason Ferroelec Freq Contr 45,* 84-97 (1998).

27. Lu JY. Transmit-receive dynamic focusing with limited diffraction beams, in *1997 IEEE Ultrason Symp Proc,* vol. 2, pp. 1543-1546 (IEEE Catalog no. 97CH36118, 1997) (ISSN: 1051-0117).

28. Lu JY, Cheng J, Wang J. High frame rate imaging system for limited diffraction array beam imaging with square-wave aperture weightings, *IEEE Trans Ultrason Ferroelec Freq Contr 53,* 1796-1812 (2006).

29. Cheng J, Lu JY. Fourier based imaging method with steered plane waves and limited-diffraction array beams, in *2005 IEEE Ultrason Symp Proc,* vol. 2, pp. 1976-1979 (IEEE Cat. no. 05CH37716C, 2005) (ISSN: 1051-0117).

30. Cheng J, Lu JY. Extended high frame rate imaging method with limited diffraction beams, *IEEE Trans Ultrason Ferroelec Freq Contr 53,* 880-899 (2006).

31. Lu JY. Limited diffraction array beams, *Int J Imag Syst Tech 8,* 126-136 (1997).

32. Lu JY. Improving accuracy of transverse velocity measurement with a new limited diffraction beam, in *1996 IEEE Ultrason Symp Proc,* pp. 1255-1260 (IEEE Cat. no. 96CH359932, 1996) (ISSN: 1051-0117).

33. Lu JY, He S. Increasing field of view of high frame rate ultrasonic imaging, *in J Acoust Soc Amer 107,* p. 2779 (2000) (abstract).

34. Lu JY. Nonlinear processing for high frame rate imaging, *J Ultrasound Med, vol. 18,* no. 3 (Supplement), p. S50, (1999) (abstract).

35. Soumekh M. Array imaging with beam-steered data, *IEEE Trans Image Proc 1,* 379-390 (1992).

36. Lu JY, Wang J. Square-wave aperture weightings for reception beam forming in high frame rate imaging, in *2006 IEEE Ultrason Symp Proc,* vol. 1, pp. 124-127 (IEEE Cat. no. 06CH37777, 2006) (ISSN: 1051-0117).

37. Flax SW, O'Donnell M. Phase aberration correction using signals from point reflectors and diffuse scatterers: basic principles, *IEEE Trans Ultrason Ferroelec Freq Contr 35,* 758-767 (1988).

38. Nock LF, Trahey GE, Smith SW. Phase aberration correction in medical ultrasound using speckle brightness as a quality factor, *J Acoust Soc Amer* 85, 1819-1833 (1989).

39. Freiburger PD, Sullivan DC, Leblanc BH, Smith SW, Trahey GE. Two dimensional ultrasonic beam distortion in the breast: in vivo measurements and effects, *Ultrasonic Imaging 14,* 398-414 (1992).

40. Rachlin D. Direct estimation of aberrating delays in pulse-echo imaging systems, *J Acoust Soc Amer 88,* 191-198 (1990).

41. Ng GC, Worrell SS, Freiburger PD, Trahey GE. A comparative evaluation of several algorithms for phase aberration correction, *IEEE Trans Ultrason Ferroelec Freq Contr 41,* 631-643 (1994).

42. O'Donnell M. Coded excitation system for improving the penetration of real-time phased-array imaging systems, *IEEE Trans Ultrason Ferroelec Freq Contr 39,* 341-351 (1992).

43. Shen J, Wang H, Cain C, Ebbini ES. A post-beamforming processing technique for enhancing conventional pulse-echo ultrasound imaging contrast resolution, in *1995 IEEE Ultrason Symp Proc,* vol. 2, pp. 1319-1322 (IEEE Cat. no. 95CH35844, 1995).

44. Aussel JD, Monchalin JP. Structure noise reduction and deconvolution of ultrasonic data using wavelet decomposition, in *1989 IEEE Ultrason Symp Proc,* pp. 1139-1144 (1989).

45. Lu JY, He S. Effects of phase aberration on high frame rate imaging, *Ultrasound Med Biol 26,* 143-152 (2000).

46. Lu JY. A study of signal-to-noise ratio of the Fourier method for construction of high frame rate images, in *Acoustical Imaging 24,* pp. 401-405 (2000).

47. Steinberg BD. Digital beamforming in ultrasound, *IEEE Trans Ultrason Ferroelec Freq Contr 39,* 716-721 (1992).

48. Lu JY, Waugaman JL. Development of a linear power amplifier for high frame rate imaging system, in *2004 IEEE Ultrason Symp Proc,* vol. 2, pp. 1413-1416 (IEEE Cat. no. 04CH37553C, 2004) (ISSN: 1051-0117).

49. Lu JY. A multimedia example, *IEEE Trans Ultrason Ferroelec Freq Contr 50,* 1078 (2003).

50. Kak AC, Slaney M. *Principle of Computerized Tomographic Imaging,* Ch. 6 (New York, NY: IEEE Press, 1987).

51. Born M, Wolf E. *Principles of Optics,* 7th ed., Ch. 13 (Cambridge: Cambridge University Press, 1999).

52. Kino CS. *Acoustic Waves: Devices, Imaging and Analog Signal Processing* (Englewood Cliffs, N.J.: Prentice-Hall, 1987).

53. Bracewell R. *The Fourier Transform and its Applications,* Chs. 4 and 6 (New York: McGraw-Hill, 1965 ).

54. Wang J, Lu JY. Motion artifacts of extended high frame rate imaging, *IEEE Trans Ultrason Ferroelec Freq Contr 54,* 1303-1315 (2007).